CrossMark

J. Fluid Mech. (2016), *vol.* 787, *pp.* 237–253. © Cambridge University Press 2015
doi:10.1017/jfm.2015.691

The turbulent wall plume from a vertically distributed source of buoyancy

Craig D. McConnochie[1,†] **and Ross C. Kerr**[1]

[1]Research School of Earth Sciences, The Australian National University, Canberra, ACT 2601, Australia

(Received 10 March 2015; revised 11 November 2015; accepted 18 November 2015;
first published online 15 December 2015)

We experimentally investigate the turbulent wall plume that forms next to a uniformly distributed source of buoyancy. Our experimental results are compared with the theoretical model and experiments of Cooper & Hunt (*J. Fluid Mech.*, vol. 646, 2010, pp. 39–58). Our experiments give a top-hat entrainment coefficient of 0.048 ± 0.006. We measure a maximum vertical plume velocity that follows the scaling predicted by Cooper & Hunt but is significantly smaller. Our measurements allow us to construct a turbulent plume model that predicts all plume properties at any height. We use this plume model to calculate plume widths, velocities and Reynolds numbers for typical dissolving icebergs and ice fronts and for a typical room with a heated or cooled vertical surface.

Key words: convection in cavities, plumes/thermals, turbulent convection

1. Introduction

Uniformly distributed sources of buoyancy exist in a variety of geophysical and industrial settings. In many of these settings the flow is enclosed at the top or bottom of the buoyancy source.

There have been numerous attempts to model plumes from distributed buoyancy sources in a variety of configurations. These studies have typically been interested in building ventilation and allowed for volume fluxes through the bottom and top boundaries. Both line sources of buoyancy (Linden, Lane-Serff & Smeed 1990; Gladstone & Woods 2014) and wall sources of buoyancy (Chen, Li & Mahoney 2001; Wells & Worster 2008; Cooper & Hunt 2010) have been investigated. In addition, Baines (2002) studied the behaviour of a wall plume flowing from a two-dimensional buoyancy source into a stratified ambient. Of these, the study of Cooper & Hunt (2010) is the most relevant to the current study, as it involved two-dimensional plumes with a solid wall acting as the buoyancy source and included experiments without a ventilation flow through the top and bottom boundaries.

Cooper & Hunt (2010) developed a theoretical model that describes the turbulent plume that forms next to the buoyancy source and the stratification that develops in the interior over time. The primary motivation for their model was natural ventilation within a building where a wall or window has a different temperature from the air

†Email address for correspondence: craig.mcconnochie@anu.edu.au

https://doi.org/10.1017/jfm.2015.691 Published online by Cambridge University Press

in the room. Within this context they were particularly interested in the stratification that developed over time, and they conducted experiments to test the predicted stratification.

Wells & Worster (2008) examined the natural convection boundary layer that forms next to an isothermal surface. Theoretical analysis resulted in identical scaling for the plume width and velocity as in the model developed by Cooper & Hunt (2010) but with significantly different values for the various parameters and coefficients.

Kerr & McConnochie (2015) showed that, when a vertical ice wall dissolves into homogeneous salty water, the dissolution rate is uniform with height in the turbulent section of the plume. This dissolving ice is equivalent to a uniformly distributed source of buoyancy, where the fresh meltwater is positively buoyant compared to the salty ambient.

In this paper, we conduct experiments similar to those conducted by Kerr & McConnochie (2015) to test the models of Cooper & Hunt (2010) and Wells & Worster (2008). In particular, we aim to test the proposed scaling and determine the values of the relevant parameters and coefficients. We use the filling box predictions to calculate an entrainment coefficient and the shadowgraph particle tracking velocimetry (PTV) technique to measure the maximum plume velocity up the wall.

In § 2 we present the previously developed models of this flow and in § 3 we describe our experiments. In §§ 4 and 5 we present the results from our filling box and velocity experiments, respectively. In § 6 we use our results to present an updated plume model. Finally, in § 7 we use this model to predict plume widths, velocities and Reynolds numbers next to dissolving icebergs and heated or cooled vertical surfaces in buildings.

2. Past theoretical modelling

2.1. *The filling box model of Cooper & Hunt*

The theoretical model of Cooper & Hunt (2010) describes a turbulent wall plume with a vertically distributed source of buoyancy. They use an approach that is similar to that of Morton, Taylor & Turner (1956) for point sources of buoyancy. The model assumes top-hat profiles of all plume quantities and is based on a symmetric line plume. It does not include any viscous effects and predicts a velocity maximum immediately next to the wall. The height of the laminar portion of the boundary layer is also assumed to be negligible.

The model predicts that, for a turbulent wall plume in a uniform ambient fluid, the following relationships exist for the plume buoyancy flux, F, top-hat width, b_P, vertical velocity, w_P, buoyancy, Δ_P, volume flux, Q_P, and momentum flux, M_P:

$$F = \Phi z, \tag{2.1}$$

$$b_P = \tfrac{3}{4}\alpha_P z = C_1 z, \tag{2.2}$$

$$w_P = \left(\tfrac{4}{5}\right)^{1/3} \alpha_P^{-1/3} \Phi^{1/3} z^{1/3} = C_2 \Phi^{1/3} z^{1/3}, \tag{2.3}$$

$$\Delta_P = \tfrac{4}{3}\left(\tfrac{5}{4}\right)^{1/3} \alpha_P^{-2/3} \Phi^{2/3} z^{-1/3} = C_3 \Phi^{2/3} z^{-1/3}, \tag{2.4}$$

$$Q_P = \tfrac{3}{4}\left(\tfrac{4}{5}\right)^{1/3} \alpha_P^{2/3} \Phi^{1/3} z^{4/3} = C_4 \Phi^{1/3} z^{4/3}, \tag{2.5}$$

$$M_P = \tfrac{3}{4}\left(\tfrac{4}{5}\right)^{2/3} \alpha_P^{1/3} \Phi^{2/3} z^{5/3} = C_5 \Phi^{2/3} z^{5/3}, \tag{2.6}$$

where C_1–C_5 are all constants, α_P is the entrainment coefficient defined as the ratio between w_P and the velocity with which ambient water is drawn into the plume,

https://doi.org/10.1017/jfm.2015.691 Published online by Cambridge University Press

Φ is the buoyancy flux per unit area, z is the distance in the direction of flow, and $\Delta_P = g(\rho_e - \rho)/\rho_1$ where ρ_e is the ambient fluid density, ρ is the density of the plume and ρ_1 is a reference density.

Equation (2.5) can be integrated to model the propagation of the first front through the ambient fluid enclosed in a filling box. This gives the location of the first front, as defined by Baines & Turner (1969), as

$$\frac{z_0}{H} = \left[1 + \frac{1}{3} C_4 W^{-1} H^{1/3} \Phi^{1/3} t\right]^{-3}, \tag{2.7}$$

where W is the width of the tank measured perpendicularly to the distributed source, H is the height of the buoyancy source, and t is the time since the buoyancy source was activated. This prediction was compared to experiments, but no other part of the model has been validated.

The experiments of Cooper & Hunt (2010) used a porous plate as one endwall through which a saline solution was forced. It is noted that this technique did not produce a perfectly uniform buoyancy flux due to the increase in hydrostatic pressure across the plate with increasing depth. This technique also requires a volume flux from the wall, which would not be present in the case of a heated or cooled surface inside a building. This volume flux results in an advective boundary layer, while the boundary layers found next to heated or cooled walls, and dissolving ice shelves or icebergs, will be diffusive. An advective boundary layer at a large Péclet number will have a sharp change in density, while a diffusive boundary layer will have a more gradual density profile.

2.2. *The boundary layer model of Wells & Worster*

Wells & Worster (2008) developed a model for the natural convection boundary layer that forms next to an isothermal surface. On the scale of walls in buildings and our experiments, they describe a turbulent flow regime where the laminar sublayer is dominated by its own buoyancy. In this regime they predict that the Nusselt number (the ratio of convective heat transfer to conductive heat transfer) will scale as the one-third power of the Rayleigh number (the ratio of buoyancy and viscous forces), giving a plume width, b, and velocity, w, of

$$b = \tfrac{3}{4} E_2 z, \tag{2.8}$$

$$w = \left[\frac{4\beta_1}{5E_2(1+\beta_1)(Pr\,Ra_c)^{1/3}}\right]^{1/3} (g'\kappa)^{1/9}(g'z)^{1/3}, \tag{2.9}$$

where β_1 is a constant, E_2 is the entrainment coefficient, which they estimate as 0.135, Pr is the Prandtl number, Ra_c is a critical Rayleigh number where the outer flow becomes turbulent, g' is the reduced gravity of the plume and κ is the thermal diffusivity. Within this regime, the same $w \sim z^{1/3}$ scaling exists as in the model of Cooper & Hunt (2010).

Wells & Worster (2008) predict a transition to another turbulent regime where the Nusselt number scales as the one-half power of the Rayleigh number. Within this regime, the laminar sublayer is no longer driven by its own buoyancy and is instead driven by the shear imposed on it. For thermal convection next to heated surfaces, the transition to this regime is expected to occur at $Ra \sim 10^{16}$, while for compositional convection in the ocean, the transition is expected to occur at $Ra \sim 10^{21}$

https://doi.org/10.1017/jfm.2015.691 Published online by Cambridge University Press

(Kerr & McConnochie 2015). This would require heights much larger than typical building heights in air and hundreds of metres next to ice shelves and icebergs in the ocean. Thus, the buoyancy-driven regime and not the shear-driven regime is of key interest in relation to both building ventilation and Antarctic ice dissolution.

3. Experiments

We have conducted a series of experiments to test the predicted velocity from (2.3) and the first front propagation of (2.7). Similarly to the experiments of Cooper & Hunt (2010), measurement of the first front position, combined with (2.7), is used to obtain an entrainment coefficient. By measuring both the first front propagation and the maximum plume velocity, we were able to quantify all top-hat plume properties at any point in the plume.

The experiments were conducted in a 1.2 m high, 1.5 m wide and 0.2 m long tank kept in a temperature-controlled room. Ice was grown from fresh water against one endwall and then exposed to salty water. The temperature and the salinity of the far field were varied to achieve different buoyancy fluxes, Φ, in different experiments. Buoyancy fluxes in the range $\Phi = (1.9\text{–}6.4) \times 10^{-7}$ m^2 s^{-3} were achieved, giving Rayleigh numbers of $(3.6\text{–}8.9) \times 10^{13}$.

Figure 1 shows photographs of an experiment with the flow visualised using the shadowgraph technique. The apparatus and experimental method are fully described in Kerr & McConnochie (2015). Kerr & McConnochie (2015) found that, when an ice wall dissolves into homogeneous salty water, the dissolution rate is uniform in the turbulent section of the flow. This behaviour corresponds to a uniformly distributed buoyancy flux and provides a convenient mechanism for testing (2.1)–(2.6).

The position of the first front was measured using a conductivity–temperature probe that traversed vertically through the far field. Typical profiles of salinity and temperature are shown in figure 2. The first front measurement was based on the salinity profile, as it had a sharper first front due to the slower diffusion of salt compared to heat. Conductivity and temperature measurements were taken on the downward traverse to minimise the effect of mixing in the wake of the probe.

Velocity measurements were made using a shadowgraph PTV technique. This technique is very similar to the schlieren particle image velocimetry (PIV) technique described by Jonassen, Settles & Tronosky (2006) with shadowgraph used instead of schlieren. It is also similar to the technique described in Crone, McDuff & Wilcock (2008), although they used a significantly different method to compute velocity fields. All of these methods represent an adaptation of traditional PTV or PIV techniques in which turbulent eddies are tracked instead of traditional particles. The PTV software 'Streams' (Nokes 2014) was used for feature identification, particle matching and the computation of velocity fields.

For shadowgraph PTV we used a zoomed-in camera window compared to figure 1. This provided higher resolution of turbulent features and enabled more accurate feature identification. An example of a shadowgraph PTV frame is shown in figure 3. The flow was filmed for approximately 10 s at each height and the resulting velocity fields were time-averaged. Averaging over longer periods of time was tested but did not change the results.

The flow that we observed was very similar to the compressible turbulent boundary layer flow that Jonassen *et al.* (2006) investigated. Both flows have similar strengths and weaknesses regarding the use of shadowgraph PTV or schlieren PIV. Since both flows are primarily two-dimensional, the shadowgraph method provides an

https://doi.org/10.1017/jfm.2015.691 Published online by Cambridge University Press

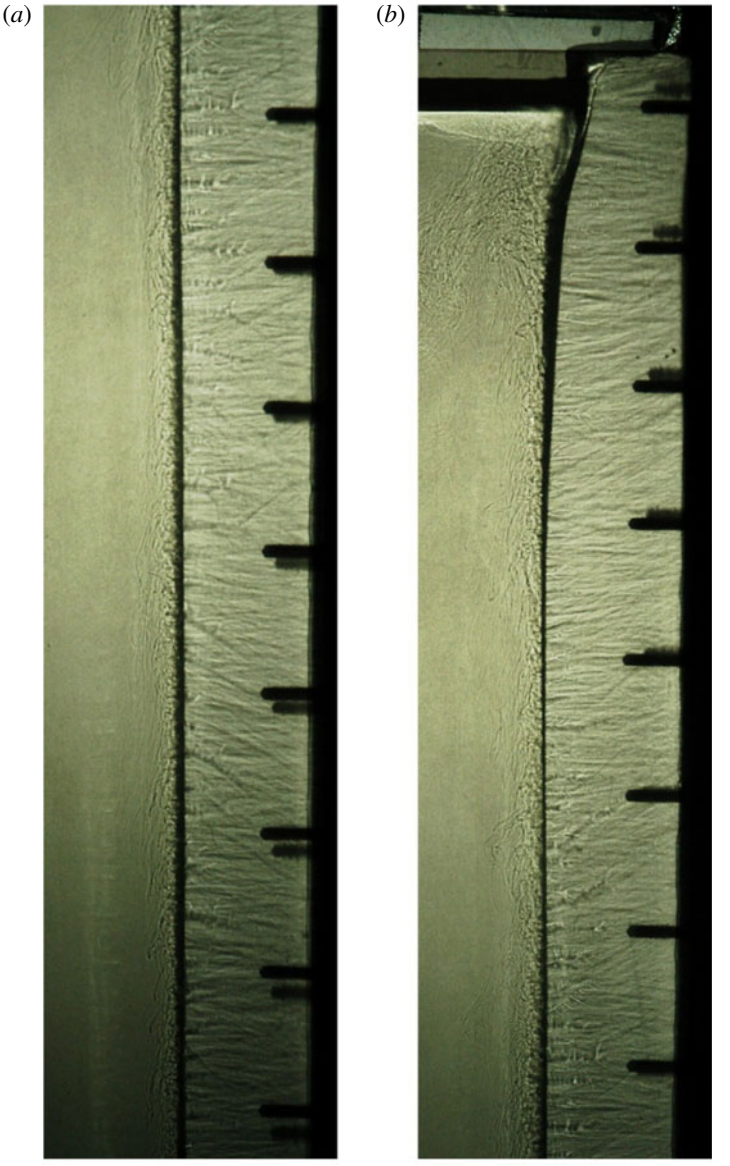


FIGURE 1. The wall plume visualised using the shadowgraph method with ice on the right and the salt water ambient on the left of each image. These photographs were presented in Kerr & McConnochie (2015) and were taken from a qualitative experiment with a far-field temperature of 3.9 °C and salinity of 3.31 wt% NaCl. The vertical spacing of the black screws in the side walls is 6 cm. The photos show (*a*) the ice from a height of 32 cm up to 76 cm, and (*b*) the ice from a height of 72 cm to the free surface at 114 cm.

easily interpretable representation of the flow, which would not be true if there was significant flow variation through the light path.

Since the flow was highly turbulent, there were many eddies that could be tracked, giving the equivalent of an appropriate seeding density of particles in traditional PTV or PIV. However, near the edge of our rising plume, this ceased to be true. At the

https://doi.org/10.1017/jfm.2015.691 Published online by Cambridge University Press

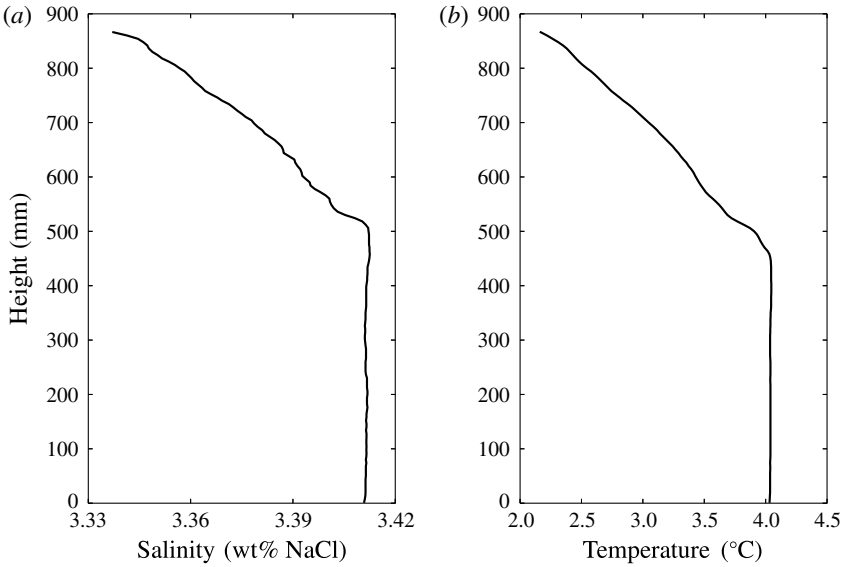


FIGURE 2. Examples of a salinity and temperature profile made during an experiment. These particular profiles were made after 40 min and the experiment had a far-field temperature of 4.1 °C, a far-field salinity of 3.41 wt% NaCl and a buoyancy flux of $\Phi = 4.0$ m^2 s^{-3}.

edge of the plume there were intermittent eddies, but these were not sufficient for shadowgraph PTV to be reliable. This was obviously also true in the quiescent far field. Finally, very near to the wall we were not able to properly resolve the eddies due to the refraction of light through the tank and the reflection of light off the ice. Within these limitations, we were able to obtain a reliable velocity profile around the location of maximum velocity. The velocity maximum was accurately measured and is the key feature of our investigation.

The buoyancy flux was defined as

$$\Phi = V\frac{\rho_s}{\rho_w}\frac{g(\rho_f - \rho_w)}{\rho_f}(1 - \mathscr{R}^{-1}), \tag{3.1}$$

where V is the measured dissolving velocity of the ice, ρ_s is the density of the ice, ρ_w is the density of fresh water at 0 °C, ρ_f is the far-field density, g is the acceleration due to gravity and $\mathscr{R}$ is the ratio of compositional to thermal buoyancy, defined as in Kerr & McConnochie (2015) as

$$\mathscr{R} = \frac{\beta S_f}{\alpha_{exp}[\rho_w L_i + \rho_i c_i (T_{iw} - T_i)]/\rho_f c_f}, \tag{3.2}$$

where α_{exp} is the thermal expansion coefficient, β is the equivalent coefficient for salt, S_f and c_f are the salinity and specific heat of the far field, L_i, ρ_i, c_i and T_i are the latent heat, density, heat capacity and temperature of the ice, and T_{iw} is the temperature at the ice–water interface. The value of T_{iw} was calculated using the turbulent dissolution model of Kerr & McConnochie (2015).

https://doi.org/10.1017/jfm.2015.691 Published online by Cambridge University Press

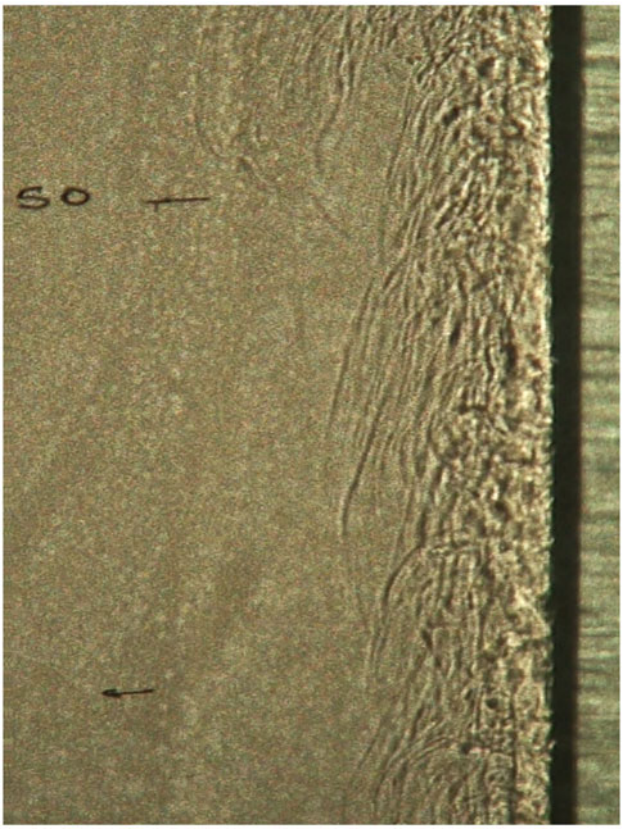


FIGURE 3. A shadowgraph image of the wall plume as used for velocity measurement. The two black horizontal lines are 5 cm apart and the upper line is 50 cm above the base of the tank. The experiment had a far-field temperature of 4.3 °C and salinity of 1.94 wt% NaCl. The ice–water interface is at the left edge of the thick dark shadow and the ice is to the right.

The correction $(1-\mathscr{R}^{-1})$ is necessary since the compositional and thermal buoyancy act in opposing directions. By assuming that both buoyancy sources are well mixed inside the turbulent plume, the interaction is simplified.

It is possible that the combination of compositional and thermal buoyancy fields could lead to double-diffusive convection in this system. This has not been explicitly tested for but no evidence of double-diffusive convection was observed in these experiments. In the case of ice melting into a stratified ambient, double diffusion can result in horizontal intrusions (Huppert & Josberger 1980; Huppert & Turner 1980) but this has not been observed in the case of a homogeneous ambient.

Measurements of the dissolving velocity, V, have a standard deviation with height of 6 %. The far-field temperature and salinity, T_f and C_f, are known to the nearest 0.1 °C and 0.1 wt% NaCl, respectively. This uncertainty in far-field conditions translates to a maximum uncertainty in $(\rho_f-\rho_w)$ of 3 % and in $(1-\mathscr{R}^{-1})$ of approximately 6 %. All other constants in (3.1) have insignificant amounts of uncertainty. This translates to a 9 % uncertainty in the values of Φ.

https://doi.org/10.1017/jfm.2015.691 Published online by Cambridge University Press

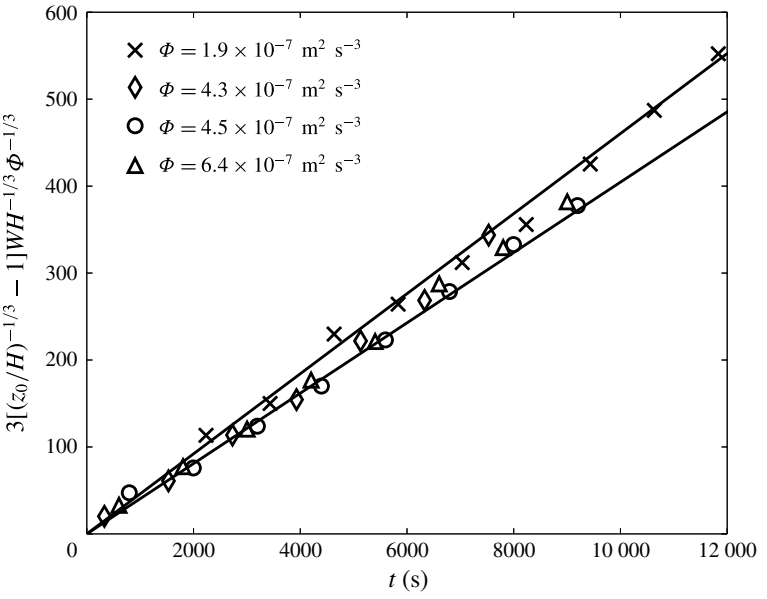


FIGURE 4. The propagation of the first front throughout an experiment. The slope represents C_4, with the two solid lines representing an entrainment coefficient of $\alpha_P = 0.014$ and $\alpha_P = 0.017$ or a volume flux coefficient of $C_4 = 0.040$ and $C_4 = 0.046$.

4. First front measurements

We use the propagation of the first front with time to estimate a value of the entrainment coefficient, α_P, defined as in the model of Cooper & Hunt (2010). Equation (2.7) has been used to produce a quantity that depends linearly on time as shown in (4.1):

$$3\left[\left(\frac{z_0}{H}\right)^{-1/3} - 1\right] WH^{-1/3}\Phi^{-1/3} = C_4 t. \tag{4.1}$$

In figure 4 the left-hand side of (4.1) is plotted against time since the start of the experiment for four experiments with different buoyancy fluxes, Φ. Figure 4 is then used to estimate the volume flux constant, C_4. The data in figure 4 have been shifted to force the curves through the origin. In the original data there were small offsets caused by a limited amount of dissolution before the experiment was started and by the conductivity profiles not being started at the exact start of the experiment. This offset was typically less than 300 s.

Table 1 gives the value of the volume flux constant, C_4, as obtained from figure 4, along with the far-field conditions, the value of $\mathscr{R}$ and a computed entrainment coefficient, α_P, as defined in (2.5). As shown in figure 4 and table 1, we measure an entrainment coefficient of 0.014–0.017. This value is comparable with but smaller than that reported in Cooper & Hunt (2010) of 0.02–0.03. The observed entrainment coefficient will be redefined in § 6, using the velocity measurements described in § 5, such that the relationship $\mathrm{d}Q/\mathrm{d}z = \alpha w$ is observed.

Our experiments are slightly different from those of Cooper & Hunt (2010), which could result in our reduced entrainment coefficient. The most significant difference is that, in their experiments, salty water was forced through a semipermeable membrane into still ambient fluid. This contrasts with our experiments, where the

https://doi.org/10.1017/jfm.2015.691 Published online by Cambridge University Press

Φ ($m^2\ s^{-3}$)	T_f (°C)	C_f (wt% NaCl)	V ($\mu m\ s^{-1}$)	$\mathscr{R}$ —	C_4 —	α_P —
1.9×10^{-7}	1.3	3.2	1.09	5.7	0.0458	0.0169
4.3×10^{-7}	3.7	2.9	2.70	6.2	0.0420	0.0148
4.5×10^{-7}	4.1	3.4	2.47	5.5	0.0407	0.0141
6.4×10^{-7}	3.7	4.1	2.99	4.9	0.0424	0.0150

TABLE 1. Volume flux coefficients, C_4, entrainment coefficients, α_P, and ratio of compositional to thermal buoyancy, $\mathscr{R}$, from first front data for four different buoyancy fluxes.

buoyancy diffused away from a very slowly retreating interface as the ice dissolved (measurements of the maximum plume velocity were typically around 5000 times larger than the dissolution velocity). The diffusive interface would have resulted in a gradual buoyancy profile across the laminar sublayer, while the advection at high Péclet number in the experiments of Cooper & Hunt (2010) would have resulted in a sharp change in buoyancy at the edge of the laminar sublayer.

We define a Péclet number as $V_o/(\kappa_c/h_c)$, where V_o is the advection velocity from the experiments of Cooper & Hunt (2010), κ_c is the diffusion coefficient of salt and h_c is the thickness of the diffusive compositional boundary layer as defined by Kerr & McConnochie (2015). This Péclet number is the ratio between advective and diffusive transport through the diffusive compositional boundary layer. For our experiments $V_o = 0$ so the Péclet number is also 0 and there is no advective transport through the compositional boundary layer. For the experiments of Cooper & Hunt (2010), however, the Péclet number is much larger than 1 (approximately 20 and 40 for their two buoyancy fluxes). Since this Péclet number is much larger than 1, the advection of salt will dominate the diffusion of salt through the laminar sublayer, and a sharp change in buoyancy is expected from the laminar sublayer to the turbulent plume. In contrast, our experiments should result in a gradually increasing salinity through the sublayer and into the plume.

Our apparatus could have resulted in more of the buoyant fluid being trapped near the wall than in the apparatus of Cooper & Hunt (2010). Trapping buoyant fluid near the wall could decrease the ability of the plume to entrain ambient water as the high-velocity fluid would also be trapped near the wall. We note that a diffusive interface will be present in both the case of room ventilation and the dissolution of Antarctic ice shelves and icebergs.

4.1. *Stratification above the first front*

In addition to the position of the first front, the conductivity–temperature probe also regularly measured the stratification that formed above the first front. Figure 5 shows the stratification that develops with time during an experiment.

The stratification that develops is approximately linear for most of the height above the first front. As the first front propagates down the tank, the stratification appears to weaken slightly. This approximately linear stratification with continuous buoyancy across the first front has been observed in many previous studies of turbulent plumes from distributed sources (Linden *et al.* 1990; Chen *et al.* 2001; Cooper & Hunt 2010; Gladstone & Woods 2014). Despite the strong experimental evidence that the buoyancy profile is continuous at the first front and approximately linear above it,

https://doi.org/10.1017/jfm.2015.691 Published online by Cambridge University Press

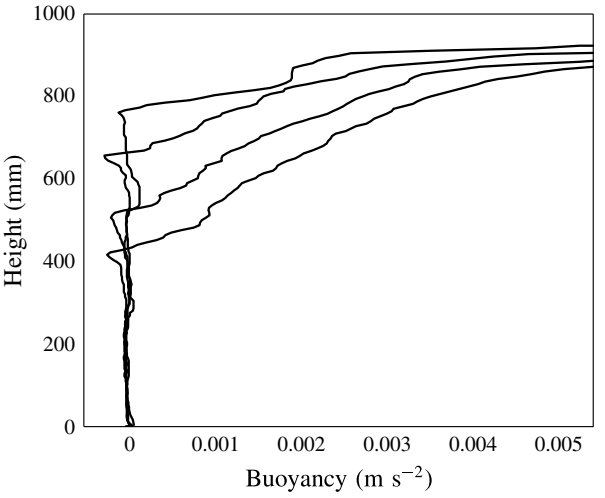


FIGURE 5. Buoyancy profiles as measured by the conductivity–temperature traverser, showing the development of stratification above the first front with time. The profiles were taken 20, 40, 60 and 80 min after the start of the experiment, with the first front getting progressively lower over this time. Buoyancy is calculated as $g(\rho_e - \rho)/\rho_e$, where ρ_e is the ambient density below the first front and ρ is the measured density.

many attempts at modelling these flows result in a step change in buoyancy at the first front and a nonlinear buoyancy profile above it (Linden *et al.* 1990; Cooper & Hunt 2010). The discrepancy between experimental results and model predictions appears to be caused by a lack of detrainment in models. Without some mechanism for detrainment, a continuous buoyancy profile across the first front is not possible, which suggests that detrainment into the stratified interior is an important process in these plumes that must be included in any modelling efforts.

5. Velocity measurements

Figure 6 shows our measurements of maximum plume velocity plotted against distance from the turbulent transition, $z - Z_{turb}$, where Z_{turb} is the height where the plume becomes turbulent. The turbulent transition was typically between 10 and 15 cm from the base of the tank and the measured values are shown in table 2. The velocity measurements are scaled by $\Phi^{-1/3}$ so that the dependence on the buoyancy flux is clearly shown. Figure 6 shows that the velocity approximately follows the $w \sim \Phi^{1/3}$ scaling predicted by (2.3).

Figure 7 shows the logarithm of the data on figure 6 separated by experiment. On figure 7 the lines represent the $w \sim z^{1/3}$ scaling relationship predicted by (2.3) and (2.9). The data are consistent with this height scaling over the entire range of heights and buoyancy fluxes that were examined.

There was a small vertical volume flux through the turbulent transition so a virtual source that would be located at some point between the base of the tank and the turbulent transition should be used instead of Z_{turb}. However, the strong agreement between the data plotted on figure 7 and the predicted $w \sim z^{1/3}$ scaling suggests that the virtual source is very close to the turbulent transition. There may be a small Φ dependence on figure 6. The experiments performed at lower values of Φ could

https://doi.org/10.1017/jfm.2015.691 Published online by Cambridge University Press

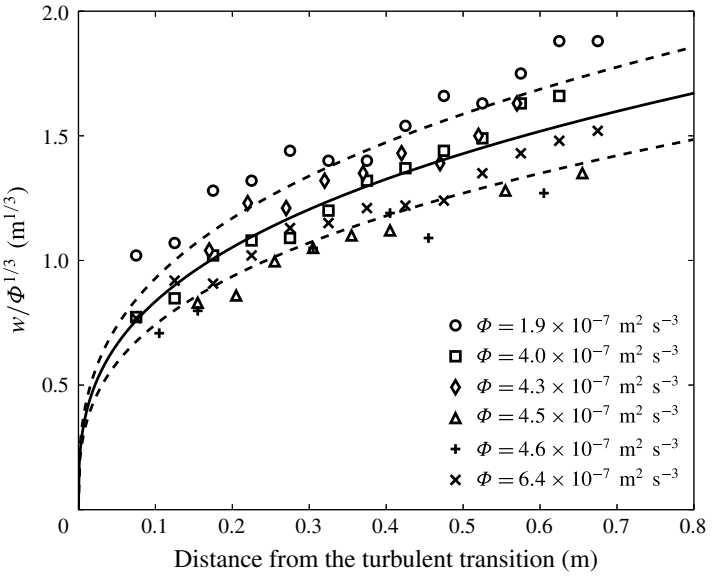


FIGURE 6. Scaled maximum velocity measurements for all six experiments. The solid line shows $w = 1.8\Phi^{1/3}z^{1/3}$ and the dashed lines show an uncertainty of one standard deviation. It is seen that the $w \sim \Phi^{1/3}$ scaling predicted by Wells & Worster (2008) and Cooper & Hunt (2010) describes the experimental results.

Φ (m^2 s^{-3})	T_f (°C)	C_f (wt% NaCl)	V (μm s^{-1})	$\mathscr{R}$ —	Z_{turb} (cm)	$C_{2,m}$ —
1.9×10^{-7}	1.3	3.2	1.09	5.7	15	2.1 ± 0.2
4.0×10^{-7}	2.7	3.4	2.00	8.3	13	1.8 ± 0.2
4.3×10^{-7}	3.7	2.9	2.70	6.2	7.5	1.9 ± 0.1
4.5×10^{-7}	4.1	3.4	2.47	5.5	12.5	1.5 ± 0.1
4.6×10^{-7}	3.5	3.4	2.50	5.5	12.5	1.7 ± 0.2
6.4×10^{-7}	3.7	4.1	2.99	4.9	13	1.7 ± 0.1

TABLE 2. Maximum velocity constant, $C_{2,m}$, from figure 7. Measured values are an average from all data points in figure 7. The uncertainty includes the entire range of measured values; $\mathscr{R}$ shows the ratio of compositional to thermal buoyancy in each experiment; and Z_{turb} shows the distance between the base of the tank and the turbulent transition.

involve a larger distance between the virtual source and Z_{turb}, which would explain any Φ dependence on figure 6.

Table 2 shows derived values of the velocity constant, $C_{2,m} = w\Phi^{-1/3}z^{-1/3}$, for each experiment. We measured an average value of $C_{2,m}$ across the six experiments of 1.8 ± 0.2. The velocity constant, $C_{2,m}$, relates to maximum plume values and not to the top-hat values assumed in the model of Cooper & Hunt (2010). Based on the experimental observations of Cheesewright (1968) and Vliet & Liu (1969) shown in figure 8, a linear velocity profile is a very good approximation of the turbulent natural convection plume next to a uniformly distributed buoyancy source. With a

https://doi.org/10.1017/jfm.2015.691 Published online by Cambridge University Press

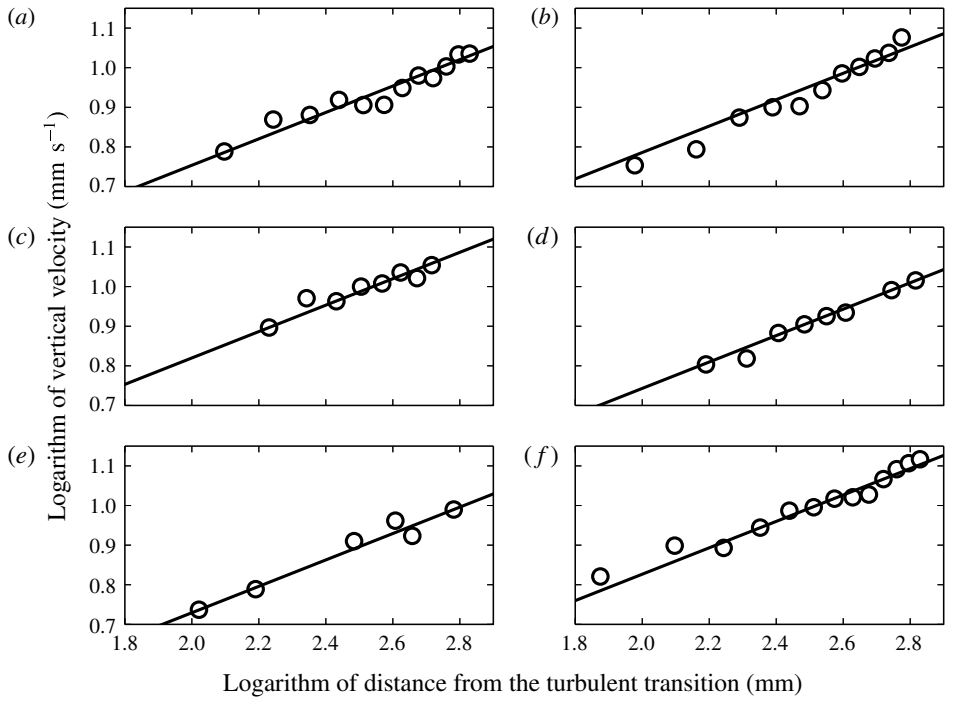


FIGURE 7. Vertical velocities for experiments at six different ambient conditions. The solid lines show the predicted $w \sim z^{1/3}$ scaling from (2.3) and (2.9): (*a*) $\phi = 1.9 \times 10^{-7}$ m^2 s^{-3}; (*b*) $\phi = 4.0 \times 10^{-7}$ m^2 s^{-3}; (*c*) $\phi = 4.3 \times 10^{-7}$ m^2 s^{-3}; (*d*) $\phi = 4.5 \times 10^{-7}$ m^2 s^{-3}; (*e*) $\phi = 4.6 \times 10^{-7}$ m^2 s^{-3}; and (*f*) $\phi = 6.4 \times 10^{-7}$ m^2 s^{-3}.

linear velocity profile, a factor of 2/3 is required to convert from a maximum velocity to a top-hat velocity such that both volume and momentum fluxes are conserved. The conversion from top-hat to physically realistic plume profiles is more fully explained in § 6. Our measurement of the top-hat value of C_2 is therefore 1.2 ± 0.1. The model of Cooper & Hunt (2010) predicts that $C_2 \approx 3.7$, based on our observations of the unadjusted entrainment coefficient, $\alpha_P = 0.0155$, which is approximately three times our observed value.

There are several explanations for this difference, some of which also explain the smaller measured entrainment coefficient discussed in § 4. Firstly, the diffusive interface could produce lower velocities. By trapping buoyancy closer to the wall, the velocity maximum may also be shifted closer to the wall. This is consistent with the natural convection boundary layer measurements shown in figure 8 (Cheesewright 1968; Vliet & Liu 1969), which show a velocity maximum that is very close to the wall. Such a velocity profile would result in a large drag force on the plume, which would result in decreased velocities.

In addition to this, the model of Cooper & Hunt (2010) assumes that viscous effects in the boundary layer adjacent to the wall are negligible. Regardless of the velocity profile, this will not be strictly true. Viscous effects from the wall must cause a no-slip boundary condition. Because of this, we would expect the top-hat velocity to be smaller than that predicted by (2.3).

https://doi.org/10.1017/jfm.2015.691 Published online by Cambridge University Press

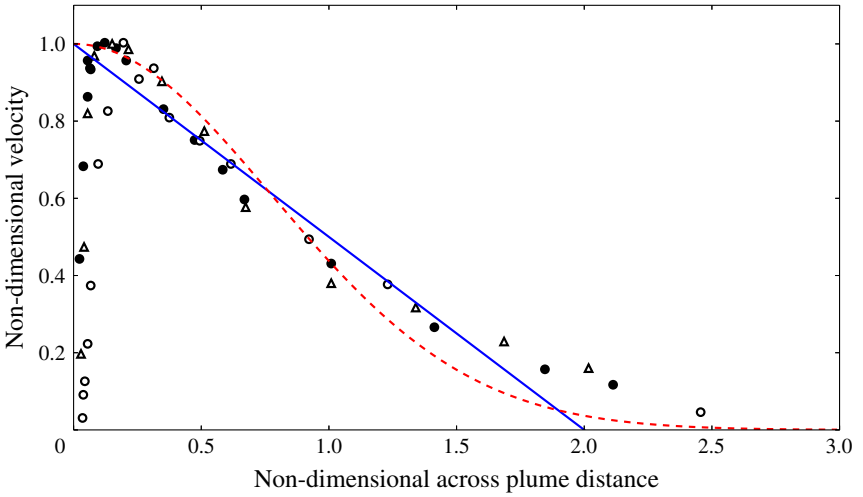


FIGURE 8. (Colour online) Vertical velocity measurements from Vliet & Liu (1969) (hollow circles and triangles) and Cheesewright (1968) (filled circles) from the rising plume next to a hot plate. Linear and Gaussian fits to the data are plotted in the blue solid line and red dashed line, respectively. The non-dimensional velocity is defined as w/w_{max} and the non-dimensional distance is defined as y/δ^*, where $\delta^* = \int_0^\infty (w/w_{max})\,\mathrm{d}y$.

6. Updated plume model

Using our measurements from §§ 4 and 5 we can construct a model for the turbulent wall plume that forms next to a vertically distributed source of buoyancy. The filling box measurements in § 4 give a volume flux, Q, of

$$Q = (0.043 \pm 0.003)\Phi^{1/3} z^{4/3}, \tag{6.1}$$

and the velocity measurements in § 5 give a maximum velocity, w, of

$$w = (1.8 \pm 0.2)\Phi^{1/3} z^{1/3}. \tag{6.2}$$

Vliet & Liu (1969) and Cheesewright (1968) measured the vertical velocity profiles in the plume next to a constant-temperature plate. Their data are shown in figure 8 with both a linear and a Gaussian fit. Unfortunately, we are unable to plot our measured velocity data on figure 8, as the non-dimensionalisation used requires the full velocity profile, which we are unable to measure. In addition, we do not have access to the dimensional data measured by Vliet & Liu (1969) or Cheesewright (1968). As such, we are unable to compare our measured velocity profiles to those presented in figure 8. The velocity measurements in figure 8 show that the velocity profile is very close to linear, with a maximum velocity close to the wall and a very sharp shear layer between the wall and the point of maximum velocity.

Based on their observations we have assumed that the velocity profile is linear, with the maximum velocity located at the wall. Appendix A copies the following analysis based on the assumption of a Gaussian velocity profile. Assuming a linear velocity profile, we can calculate the plume width, b, and momentum flux, M, as

$$b = \frac{2Q}{w} = (0.048 \pm 0.006)z \tag{6.3}$$

https://doi.org/10.1017/jfm.2015.691 Published online by Cambridge University Press

and

$$M = \frac{2Qw}{3} = (0.052 \pm 0.007)\Phi^{2/3}z^{5/3}. \tag{6.4}$$

Equations (6.1)–(6.4) form a model of all plume properties, apart from the buoyancy, derived from our measurements of volume flux and maximum plume velocity. It is possible to construct an updated top-hat model from (6.1)–(6.4) that gives the following equations for the top-hat velocity, w_T, width, b_T, and buoyancy, Δ_T:

$$w_T = \frac{2w}{3} = (1.2 \pm 0.1)\Phi^{1/3}z^{1/3}, \tag{6.5}$$

$$b_T = \frac{Q}{w_T} = (0.036 \pm 0.005)z, \tag{6.6}$$

$$\Delta_T = \frac{F}{Q} = (23 \pm 2)\Phi^{2/3}z^{-1/3}. \tag{6.7}$$

We now recalculate the top-hat entrainment coefficient, α_T, such that the equation

$$\frac{\mathrm{d}Q}{\mathrm{d}z} = \alpha_T w_T \tag{6.8}$$

is consistent with our measured velocity. An updated value of α_T is necessary, as we are not directly measuring an entrainment coefficient in § 4 but are instead measuring $Q(z)$, which also depends on the plume velocity. The original calculation of α_P was made using the plume volume flux given in (2.3). Using our measured value of w_T results in the following expression for α_T:

$$\alpha_T = \frac{1}{w_T}\frac{\mathrm{d}Q}{\mathrm{d}z} = 0.048 \pm 0.006. \tag{6.9}$$

One of the implications of our updated plume model compared with the model of Cooper & Hunt (2010) is that there must be a significant drag force acting on the plume. This drag is represented as ϵ in equation (2.1) of Cooper & Hunt (2010) and it is assumed to be negligible when formulating the solution given in our (2.1)–(2.6). By assuming negligible drag, the upwards buoyancy force was balanced by the gain in momentum flux in the plume, which led to the much larger velocity predictions than were observed in our experiments. We calculate the value of this drag as

$$\epsilon = b_T\Delta_T - \frac{\mathrm{d}M}{\mathrm{d}z} = (0.75 \pm 0.12)\Phi^{2/3}z^{2/3}, \tag{6.10}$$

which represents approximately 90 % of the upward buoyancy force. Based on the velocity profiles of Vliet & Liu (1969), such a high value does not seem unreasonable, as the velocity profile shows a maximum velocity very near to the wall, with a sharp shear zone between the wall and the velocity maximum. Such a profile would induce significant drag on the plume and result in a very high wall shear stress. Turbulent fluctuations within the plume would also cause a large amount of turbulent drag within the plume.

https://doi.org/10.1017/jfm.2015.691 Published online by Cambridge University Press

7. Physical application

We now use (6.1)–(6.3) to calculate maximum plume widths, velocities and Reynolds numbers for a typical dissolving iceberg and a typical room.

In the case of an Antarctic iceberg, we take a typical ocean temperature of 1 °C (Budd, Jacka & Morgan 1980). Following the equations of Kerr & McConnochie (2015) for ablation velocity and interface conditions, this gives a buoyancy flux, Φ, of 1.7×10^{-7} m^2 s^{-3}. Tabular icebergs in the polar oceans frequently sit several hundreds of metres deep in the water column. At a characteristic iceberg height of 200 m (Dowdeswell & Bamber 2007), the turbulent plume next to such an iceberg would have a width, b, of 9.6 ± 1.2 m, a maximum velocity, w, of 0.058 ± 0.006 m s^{-1}, and a Reynolds number, defined as $Re = Q/\nu$, where ν is the kinematic viscosity, of $(2.8 \pm 0.2) \times 10^5$. These calculations should guide any attempts to observe this rising meltwater plume in the field. In particular, it would be useful to have velocity, temperature and salinity measurements from within the plume next to an iceberg or ice front.

In the case of a room with a heat flux through a wall or window, we calculate a Rayleigh number, Ra, of 3.2×10^{10} based on a temperature difference of 10 °C between the interior and the exterior, an ambient temperature of 20 °C and a height of 3 m. For simplicity we have assumed that the buoyancy source comprises the entire height of the room to maintain a similar configuration to our experiments. For turbulent natural convection on an isothermal vertical boundary layer, the Nusselt number, Nu, is given by $Nu = 0.10Ra^{1/3}$ (Holman 2010, p. 355), which gives a Nusselt number of 317. We can use the Nusselt number to calculate a buoyancy flux as $\Phi = (Nu\kappa\Delta Tg)/(HT)$, where κ is the thermal diffusivity, ΔT is the applied temperature difference, g is gravity, H is the height of the room and T is the ambient temperature in kelvin. This gives a buoyancy flux, Φ, of 6.7×10^{-4} m^2 s^{-3}. Using this value and the maximum height of 3 m, we obtain a plume width, b, of 0.14 ± 0.02 m, a maximum plume velocity, w, of 0.23 ± 0.03 m s^{-1}, and a Reynolds number of $(1.1 \pm 0.1) \times 10^3$.

8. Conclusions

In this paper, we have presented experiments that examine the filling box that forms as a result of a vertically distributed source of buoyancy. These experiments make use of the observation of Kerr & McConnochie (2015) that ice dissolving into a homogeneous ambient will have a dissolution velocity that is constant with height when the rising plume is turbulent.

We have compared these results with the theoretical model and experiments of Cooper & Hunt (2010). We measured a top-hat entrainment coefficient based on their velocity predictions of $\alpha_P = 0.014$–0.017, which is slightly less than that measured by Cooper & Hunt (2010) of 0.02–0.03. We have also measured the maximum plume velocity with height for a variety of buoyancy fluxes. Our results agree with the model predictions of Cooper & Hunt (2010) and Wells & Worster (2008) that the velocity should scale with the one-third power of height. However, the velocities are smaller than those predicted by (2.3), which suggests that viscous drag has a significant effect on the turbulent wall plume. Using our velocity measurements we calculate a top-hat entrainment coefficient of $\alpha_T = 0.048 \pm 0.06$.

We use these observations of entrainment coefficient and velocity to produce a semi-empirical model of a turbulent wall plume with a distributed source of buoyancy. The model is applied to a typical Antarctic iceberg and a typical room, and used to

https://doi.org/10.1017/jfm.2015.691 Published online by Cambridge University Press

calculate some characteristic plume quantities for each of these physical cases. These characteristic values could be useful in planning field investigations, particularly of Antarctic icebergs, where field observations require highly specialised equipment.

Acknowledgements

We gratefully acknowledge the technical assistance of B. Tranter, T. Beasley and A. Rummery, and the financial support of the Australian Research Council Discovery Grant DP120102772. We thank three anonymous referees who provided valuable suggestions throughout the review process.

Appendix A

Here we derive equations that are the equivalents to (6.3)–(6.10) but are based upon an assumed Gaussian velocity profile:

$$w(x) = w_{max}\, \mathrm{e}^{-x^2/b^2}. \tag{A 1}$$

With this profile we have

$$b_G = \frac{2Q}{\sqrt{\pi} w_{max}} = (0.027 \pm 0.004) z \tag{A 2}$$

and

$$M_G = \frac{Qw}{\sqrt{2}} = (0.055 \pm 0.007) \Phi^{2/3} z^{5/3}. \tag{A 3}$$

We now construct a top-hat velocity, $w_{T,G}$, and width, $b_{T,G}$, based on a Gaussian velocity profile. This gives

$$w_{T,G} = \frac{w}{\sqrt{2}} = (1.3 \pm 0.1) \Phi^{1/3} z^{1/3} \tag{A 4}$$

and

$$b_{T,G} = \frac{Q}{w_{T,G}} = (0.033 \pm 0.004) z. \tag{A 5}$$

Again, we recalculate the top-hat entrainment coefficient so that $\alpha_{T,G}$ is consistent with our measured velocity, giving

$$\alpha_{T,G} = \frac{1}{w_{T,G}} \frac{\mathrm{d}Q}{\mathrm{d}z} = 0.045 \pm 0.006. \tag{A 6}$$

Finally we recalculate the drag force acting on the plume based on our Gaussian top-hat model. This gives

$$\epsilon = b_{T,G} \Delta_T - \frac{\mathrm{d}M_G}{\mathrm{d}z} = (0.67 \pm 0.11) \Phi^{2/3} z^{2/3}. \tag{A 7}$$

Equations (A 1)–(A 7) are consistent with (6.3)–(6.10) to within experimental error. Our results are somewhat insensitive to whether a linear or a Gaussian velocity profile is chosen, and previous experimental measurements (Cheesewright 1968; Vliet & Liu 1969) are not strongly convincing either way. Because of this we have used a mathematically simpler linear velocity profile throughout our main analysis.

https://doi.org/10.1017/jfm.2015.691 Published online by Cambridge University Press

REFERENCES

BAINES, P. G. 2002 Two-dimensional plumes in stratified environments. *J. Fluid Mech.* **471**, 315–337.

BAINES, W. D. & TURNER, J. S. 1969 Turbulent buoyant convection from a source in a confined region. *J. Fluid Mech.* **37**, 51–80.

BUDD, W. F., JACKA, T. H. & MORGAN, V. I. 1980 Antarctic iceberg melt rates derived from size distributions and movement rates. *Ann. Glaciol.* **1**, 103–112.

CHEESEWRIGHT, R. 1968 Turbulent natural convection from a vertical plane surface. *Trans. ASME J. Heat Transfer* **90**, 1–6.

CHEN, Z. D., LI, Y. & MAHONEY, J. 2001 Natural ventilation in an enclosure induced by a heat source distributed uniformly over a vertical wall. *Build. Environ.* **36**, 493–501.

COOPER, P. & HUNT, G. R. 2010 The ventilated filling box containing a vertically distributed source of buoyancy. *J. Fluid Mech.* **646**, 39–58.

CRONE, T. J., MCDUFF, R. E. & WILCOCK, W. S. D. 2008 Optical plume velocimetry: a new flow measurement technique for use in seafloor hydrothermal systems. *Exp. Fluids* **45**, 899–915.

DOWDESWELL, J. A. & BAMBER, J. L. 2007 Keel depths of modern Antarctic icebergs and implications for sea-floor scouring in the geological record. *Mar. Geol.* **243**, 120–131.

GLADSTONE, C. & WOODS, A. W. 2014 Detrainment from a turbulent plume produced by a vertical line source of buoyancy in a confined, ventilated space. *J. Fluid Mech.* **742**, 35–49.

HOLMAN, J. P. 2010 *Heat Transfer*, 10th edn. McGraw-Hill.

HUPPERT, H. E. & JOSBERGER, E. G. 1980 The melting of ice in cold stratified water. *J. Phys. Oceanogr.* **10** (6), 953–960.

HUPPERT, H. E. & TURNER, J. S. 1980 Ice blocks melting into a salinity gradient. *J. Fluid Mech.* **100** (2), 367–384.

JONASSEN, D. R., SETTLES, G. S. & TRONOSKY, M. D. 2006 Schlieren 'PIV' for turbulent flows. *Opt. Lasers Engng.* **44**, 190–207.

KERR, R. C. & MCCONNOCHIE, C. D. 2015 Dissolution of a vertical solid surface by turbulent compositional convection. *J. Fluid Mech.* **765**, 211–228.

LINDEN, P. F., LANE-SERFF, G. F. & SMEED, D. A. 1990 Emptying filling boxes: the fluid mechanics of natural ventilation. *J. Fluid Mech.* **212**, 309–335.

MORTON, B. R., TAYLOR, G. I. & TURNER, J. S. 1956 Turbulent gravitational convection from maintained and instantaneous sources. *Proc. R. Soc. Lond.* **234**, 1–23.

NOKES, R. 2014 Streams, version 2.03: System theory and design. Department of Civil and Natural Resources Engineering, University of Canterbury, New Zealand.

VLIET, G. C. & LIU, C. K. 1969 An experimental study of turbulent natural convection boundary layers. *Trans. ASME J. Heat Transfer* **91**, 517–531.

WELLS, A. J. & WORSTER, M. G. 2008 A geophysical-scale model of vertical natural convection boundary layers. *J. Fluid Mech.* **609**, 111–137.

https://doi.org/10.1017/jfm.2015.691 Published online by Cambridge University Press